# Electrical spin injection and detection in semimetallic Bi and Bi-Pb films

Kyoung-Il Lee,[1,2] Jong Wook Roh,[1] Joonyeon Chang,[2] Suk-Hee Han,[2] Kyung-Ho Shin,[2] Won Yong Jeung,[2] Mark Johnson,[3,*] and Wooyoung Lee[1,†]

[1]*Department of Materials Science and Engineering, Yonsei University, Seoul 120-749, Korea*

[2]*Korea Institute of Science and Technology, Seoul 136-791, Korea*

[3]*Naval Research Laboratory, Washington, DC 20375, USA*

(Received 28 January 2009; published 1 May 2009)

The spin injection technique is extended to semimetal bismuth samples in a lateral spin valve geometry. We study spin injection, diffusion, and detection in a material system where a small change in sample stoichiometry results in a large change in the electronic and spin dependent transport properties of the nonmagnetic material. Measurements of magnetoresistance, using a magnetic field applied in the sample plane, as well as the Hanle effect, using a field applied perpendicular to the sample plane, are reported. We demonstrate two remarkable results: (i) a spin diffusion length of 230 $\mu$m ($T$=2 K) in a BiPb sample with temperature dependent resistivity, $\rho(T)$, which decreases with decreasing $T$ is the longest known value in a thin film; (ii) the interfacial spin polarization is 10% in BiPb samples with decreasing $\rho(T)$ and an order of magnitude smaller (0.8%) in Bi samples where $\rho(T)$ increases with decreasing $T$.

DOI: 10.1103/PhysRevB.79.195201 PACS number(s): 72.25.Hg, 72.25.Ba, 72.25.Dc, 85.75.−d

## I. INTRODUCTION

In the field of spintronics,[1,2] spin transport involving ferromagnetic metals is highly successful in magnetic tunnel junctions (MTJs) and spin valves,[3,4] but progress toward a paradigmatic semiconductor device, such as the spin injected field-effect transistor (FET),[1,5] has been limited. Spin diffusion lengths in semiconductors are long,[6] but electrical spin injection and detection have been problematic. In a few reports of electrical spin injection and detection in semiconductors, transport effects have remained small[7] but reproducible and convincing.[8] Motivated to seek a new approach to understand the spin transport issues in semiconductors, we have extended the spin injection technique to study a nonmagnetic semimetal. Thin film samples of semimetal bismuth are characterized by a resistivity, $\rho(T)$, which increases with decreasing temperature $T$, similar to the behavior of semiconducting films, and form a first sample set. Thin films of dilute BiPb alloy are characterized by $\rho(T)$ that decreases with decreasing temperature, similar to the behavior of metallic or semimetallic films, and form a second set. Unusually long spin diffusion lengths are observed in all samples. However, the spin diffusion lengths and magnitudes of spin accumulation are very different for the two sample sets, even though the material composition is nearly the same. Our analysis shows that differences in the spin diffusion lengths can be explained by associated differences of resistivity. We also find that the spin polarization of injected current and the magnitude of spin accumulation are relatively small in the first sample set by comparison with the second set.

Bismuth is a group V semimetallic element with a highly anisotropic Fermi surface and unusual transport properties.[9,10] Transport characteristics are analyzed in a two carrier model,[11] with comparable contributions from both electrons and holes. The carrier densities in bulk Bi are small, $n \sim p \approx 3 \times 10^{17}$ cm$^{-3}$.[12] Holes have effective mass $m_h^* \approx m_e$, where $m_e$ is the free electron mass. Electrons have a lighter effective mass, $m_e^* \approx 0.1 m_e$, and relatively high mobility, $\mu_e \gg \mu_h$.[13] The carrier mean-free paths are quite long, compensating for low carrier density. The room-temperature resistivity is approximately $\rho_{\mathrm{Bi}} = 1 \times 10^{-4}$ $\Omega$ cm, roughly 50 times larger than that of most metals, even though the carrier density is smaller by $10^5$. In thin films, the resistivity $\rho = e^{-1}(n\mu_e + p\mu_h)^{-1}$ is a competition between carrier densities $n$ and $p$ and mobilities $\mu_e$ and $\mu_h$. The densities may depend on temperature and film quality, and the mobilities are very sensitive to the structural imperfections of polycrystalline films, such as grain boundaries. The temperature dependent resistivity $\rho(T)$ of Bi films may show behavior that is similar to either semiconducting or semimetallic films, with $\rho(T)$ increasing[13–15] or decreasing[16] as temperature decreases from 300 to 2 K, respectively. An alloy formed with a small amount of Pb decreases the low temperature resistivity by 1 order of magnitude. Our study uses the $Bi_{1-x}Pb_x$ material system, where $x=0$ ($x=0.05$) for two sets of thin film samples characterized by $\rho(T)$ increasing (decreasing) with decreasing $T$.

## II. EXPERIMENTS AND SAMPLE CHARACTERIZATION

The spin injection technique[17] has been used for basic research on spin dependent transport in metals for two decades and has recently seen renewed interest in the study of mesoscopic structures.[18–23] The resistance change $\Delta R = 2IR_S$ in a spin injection structure derives from spin accumulation $\tilde{M}$, a nonequilibrium population of spin polarized carriers. A ferromagnetic electrode $F1$ with magnetization **M1** injects polarized carriers into nonmagnetic sample $N$ and develops spin accumulation, which is detected as a voltage $V$ with a second ferromagnetic electrode $F2$ having magnetization **M2** [refer to Fig. 1(a)]. A hallmark of the technique is the Hanle effect, where **M1** and **M2** remain parallel, a magnetic field $H$ is applied perpendicular to the axes of the injected spins [$x$ or $z$ axes in Fig. 1(a)], the carriers precess as they diffuse, and analysis of the measured line shape $V(H)$ gives the magnitude of spin accumulation (and spin injection efficiency) and

 

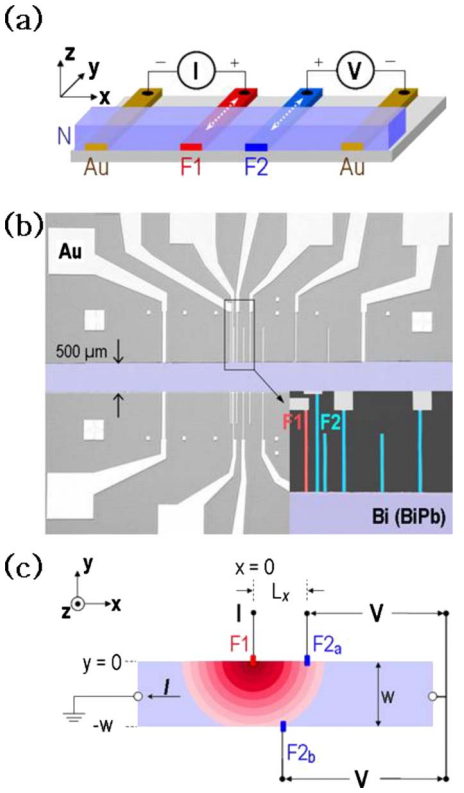


FIG. 1. (Color online) Structure of the fabricated spin injection device. (a) A schematic perspective diagram of the device. $F1$, $F2$, and $N$ denote a CoFe electrode, a NiFe electrode, and a Bi or BiPb layer, respectively. The ferromagnetic electrodes have an easy magnetization axis along $\hat{y}$. The nonlocal voltage between $F2$ and right Au electrode is measured with dc bias current applied to $F1$ as $H$ is varied. (b) Micrograph of sample Bi (26). Inset, closeup of $F1$ and $F2$ electrodes. (c) Schematic top view of a two-dimensional spin injection/detection model geometry, $w > \delta_s$. $F1$ is a spin injector and $F2_a$ ($F2_b$) is a detector located on the top (bottom) edge. Darker shading (red online) represents larger values of spin accumulation.

the transverse spin relaxation time, $T_2$. The Hanle effect was first demonstrated with a bulk Al sample[17] and has been observed in thin film samples of Nb,[24] Cu,[18] and $n$-doped GaAs.[8] In most thin film samples, the effect is undetected because of high resistivity or high spin-orbit interaction.[19–22] A second more common technique is to apply $H$ along the uniaxial anisotropy axis of $F1$ and $F2$ [$y$ axis in Fig. 1(a)] in order to manipulate **M1** and **M2** between parallel and antiparallel configurations. The $V(H)$ magnetoresistance (MR) data show dips, when **M1** and **M2** are antiparallel, having depth proportional to $\tilde{M}$. The spin diffusion length, $\delta_s = \sqrt{D\tau_s}$ (where $\tau_s$ is the mean spin lifetime and includes both transverse, $T_2$, and longitudinal, $T_1$, relaxation times[8]), is determined from measurements on several devices having different separations $L$ between injector and detector. Our study uses both the Hanle effect and MR measurements.

Spin injection studies often use a lateral spin valve structure.[17,25] In order to achieve high quality samples with reproducible resistivities, our films are relatively thick, $d \approx 9$ $\mu$m. The $N$ wire was patterned by photolithography and lift-off using a 15 $\mu$m thick photoresist, and $w$ is necessarily wide, $w = 0.5$ mm [Fig. 1(b)]. Our lateral spin valve samples therefore have the two-dimensional ($d \ll \delta_s$) geometry shown in Fig. 1(c). Bias current $I$ is injected through $F1$ at a point $x = 0$ on the top edge of $N$ and is grounded at the left end. The spin accumulation $\tilde{M}$, depicted in Fig. 1(c) with darker shading, (red online) diffuses radially from the injector and the magnitude decays exponentially with increasing distance $L$. An array of ferromagnetic detectors ($F2$) is fabricated with spacing $L_x$, as shown in the micrograph in Fig. 1(b).

Quantitatively, the voltage $IR_S$ is found to be[24]

$$R_S = \frac{\eta_1 \eta_2}{e^2} \frac{\tau_s}{N(E_F)} \frac{1}{\mathcal{V}}, \tag{1}$$

where the injector (detector) has polarization $\eta_1$ ($\eta_2$), the spacing $L$ is small, $L \ll \delta_s$, $N(E_F)$ is the density of states at the Fermi level of $N$, and $\mathcal{V}$ is the approximate sample volume occupied by $\tilde{M}$. Using an Einstein relation and a free electron expression, Eq. (1) can be written as

$$R_S = \frac{\eta_1 \eta_2 \rho \delta_s^2}{\mathcal{V}} \tag{2}$$

for the case of a simple metal. When $L$ is comparable with, or larger than, $\delta_s$, the exponential decay term appears explicitly,[24]

$$R_S = \frac{\eta_1 \eta_2 \rho \delta_s^2}{\mathcal{V}} e^{-L/\delta_s}. \tag{3}$$

Since $I$ flows to ground at the left end, the portion of the sample to the right of the injector is approximately equipotential in the nonlocal geometry.[25,26] Small portions of $I$ flow along $+\hat{x}$ for $x > 0$ at the top edge of $N$, curve along $-\hat{y}$, and then flow along $-\hat{x}$ near the bottom edge. These small currents result in voltages $V(x > 0; y = 0, -w)$ that differ from the voltage at the right end of $N$ and appear as a small baseline resistance, $R_B$, in the measurements. Measured values of $R_B$ fit well to an analytic calculation,[26] thereby justifying the use of the two-dimensional model.

The 10 $\mu$m wide injector $F1(Co_{0.84}Fe_{0.16})$ and detector $F2(Ni_{0.81}Fe_{0.19})$ are designed to exhibit distinct switching fields because of differing intrinsic coercivities and magnetic anisotropies [Fig. 1(b)]. The 25 nm thick $F1$ and $F2$ electrodes were deposited on a $SiO_2$ substrate by dc magnetron sputtering. Any oxidation on the tops of $F1$ or $F2$ was removed by an $Ar^+$ plasma etching process prior to deposition of the $N$ material. The resulting $F/N$ interface resistance is too small to measure. Since the resistance per square of $F$ is much larger than that of $N$, injection and detection can be assumed to occur at points near the edges of $N$, an assumption that is justified by detailed fits to the measured baseline resistances.[26] As a consequence, detectors located on the top (bottom) edge have radial distance $L = L_x$ ($L = \sqrt{L_x^2 + (0.5\ \text{mm})^2}$) from $x = 0$.

The 8.3 $\mu$m thick Bi and 9.2 $\mu$m thick $Bi_{0.95}Pb_{0.05}$ channel layers were deposited by rf magnetron sputtering. The $Bi_{0.95}Pb_{0.05}$ samples were characterized, after lithographic processing, by measuring the resistivities and Hall coefficients as functions of temperature. Measurements for two

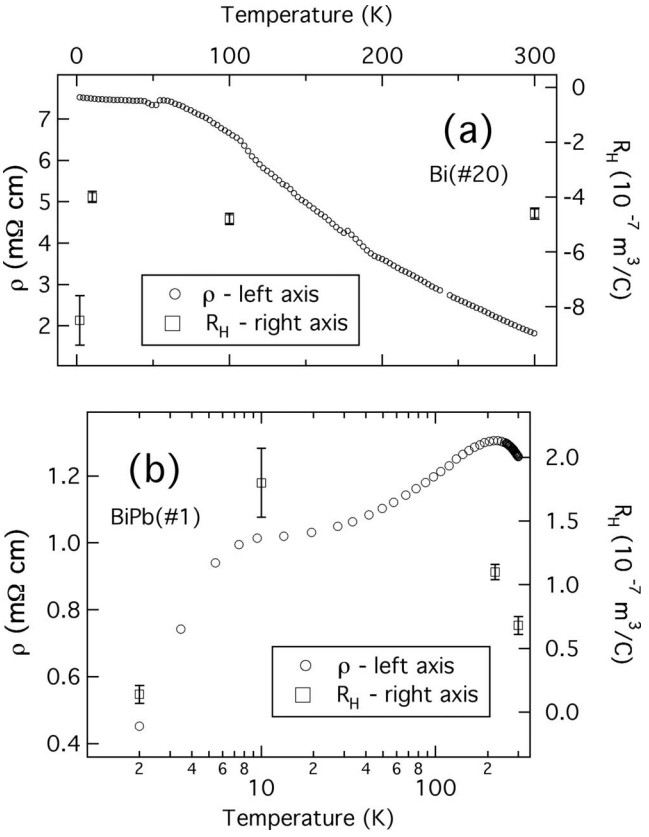


FIG. 2. Resistivity and Hall coefficient of patterned Bi and BiPb samples. (a) Sample Bi (20). (b) Sample BiPb (1).

samples, Bi (20) representing set 1 and BiPb (1) representing set 2, are shown in Figs. 2(a) and 2(b), respectively. Resistivity values at room temperature are quite comparable, $\rho_{\mathrm{Bi}}=1.8$ m$\Omega$ cm and $\rho_{\mathrm{BiPb}}=1.26$ m$\Omega$ cm. The resistivity of the Bi sample increases by a factor of about 4.2 as $T$ decreases to 2 K, whereas $\rho(T)$ of BiPb decreases by a factor of 2.8 over the sample temperature range.

An analysis of the character of our samples in a two carrier model[11] would require temperature dependent resistivity, Hall effect, ordinary magnetoresistance, and thermoelectric measurements. Our patterned samples were susceptible to thermally induced stress and did not survive more than a few cryogenic cycles. We report spin injection data that were reproducible in two or more separate cryogenic runs but were unable to perform measurements of ordinary magnetoresistance and thermoelectric properties. However, resistivity and Hall coefficient measurements can be discussed in some detail. The results of these measurements indicate that both electrons and holes contribute to charge transport in both sample sets.

The resistivity of sample Bi (20), typical of two samples in set 1 and shown in Fig. 2(a), increases with decreasing $T$ with a change in slope at about $T=60$ K. This temperature dependence is quite similar to planar polycrystalline films with thickness of 1–10 $\mu$m.[13–15] The Hall coefficient, $R_H$, was measured in fields $H<1$ T and is negative at all temperatures. The sign and magnitude of $R_H$ can be compared with values for a film with similar $\rho(T)$. For example, at $T=100$ K, $R_H(100\ \mathrm{K})=-4.6\times10^{-7}$ m$^3$/C is comparable

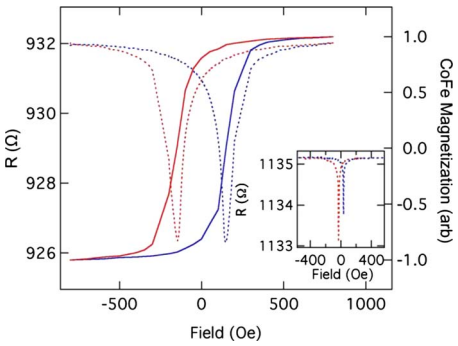


FIG. 3. (Color online) Dotted lines: AMR of $F1$, measured *in situ* with two probes (left-hand axes). Blue: field sweep up. Red: field sweep down. Solid lines: hysteresis loop of $F1$ constructed from AMR data (right hand axes). The minimal resistance value of the dips represents a state with minimal value of magnetization oriented along the $\hat{y}$ axis. Inset: AMR of $F2$.

with $R_H$ measured on a planar sputtered film of comparable thickness, $R_H(66\ \mathrm{K})=-2.7\times10^{-7}$ m$^3$/C.[13] The sign of $R_H$ indicates that electrons dominate transport, but it is not certain whether this is a result of higher density or higher mobility. The increase in the magnitude of $R_H$ by a factor of 2 between 10 and 2 K may be anomalous or may represent a decrease in carrier density, $n=1/(eR_H)$.

Figure 2(b) presents the resistivity of BiPb (1), representative of three $\mathrm{Bi}_{0.95}\mathrm{Pb}_{0.05}$ samples in set 2, in a semilogarithmic plot. A small hump appears at about $T=220$ K and a knee appears at about $T=10$ K, features that reproduced in all three samples. Quantitatively, the resistivity of sample BiPb (4) drops about 30% over the first decade (300–20 K) and then falls by 25% over the next decade (20–2 K). By comparison, the resistivity of sample BiPb (1) [Fig. 2(b)] drops about 20% over the first decade (300–20 K) and then falls by 50% over the next decade (20–2 K). The resistivity at $T=5$ K, $\rho(5\ \mathrm{K})=0.8$ m$\Omega$ cm, is a reasonable value, roughly comparable with the resistivity of a high quality polycrystalline semimetallic film of similar thickness.[27] The Hall coefficient is positive at all temperatures. The sign and magnitude of $R_H$ can be compared with values for a film with similar $\rho(T)$. For example, at $T=220$ K, $R_H(220\ \mathrm{K})=1.1\times10^{-7}$ m$^3$/C is comparable with $R_H$ measured on a single crystal film with thickness of 1.48 $\mu$m, $R_H(225\ \mathrm{K})=1.5\times10^{-7}$ m$^3$/C.[16] The sign of $R_H$ indicates that holes dominate transport. The magnitude of $R_H$ decreases by a factor of 10 between $T=10$ and 2 K.

## III. RESULTS

First discussing in-plane MR measurements, voltages are recorded as an external field $H$ is swept along the $y$ axis [refer to Fig. 1(a)]. As part of our experimental methodology, the two-probe resistance of one of the ferromagnetic electrodes is recorded simultaneously with the spin accumulation data. An example of the direct measurement of the anisotropic magnetoresistance (AMR) of $F1$ is shown as the hysteretic dotted traces in Fig. 3. A hysteresis loop for **M1** is derived from the AMR traces and is shown with solid lines.

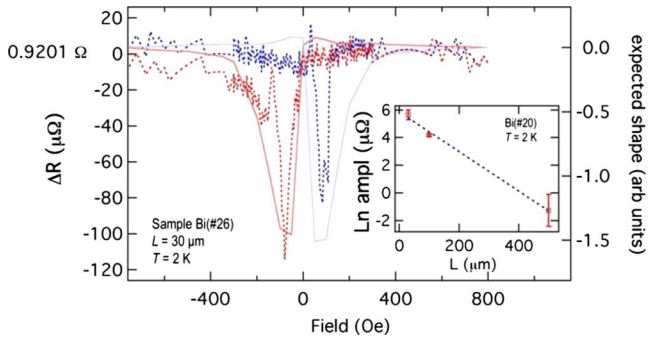


FIG. 4. (Color online) Example of spin accumulation data. Dotted lines and left-hand axis, data from sample Bi (26). $L=30$ $\mu$m. Electrodes $F1$ and $F2_a$ [refer to Fig. 1(c)]. Blue: field sweep up. Red: field sweep down. The resistance at $H=0$ is $R=0.9201$ $\Omega$, and $\Delta R$ is plotted. Solid lines and right-hand axis, shape of spin injection/detection dips as constructed from AMR data. Inset: semilogarithmic plot of $\Delta R$ as a function of $L$ for sample Bi (20).

The AMR of $F2$ was also measured (Fig. 3, inset). A feature in the nonlocal data that is associated with spin accumulation must occur when **M1** and **M2** are antiparallel. The anticipated shape, shown with the light solid lines (right-hand axis) in Fig. 4, can be derived by comparing the hysteresis loops for $F1$ and $F2$.

An example of spin injection, accumulation, and detection in a Bi film (set 1) is shown in Fig. 4. Examples of data for BiPb are shown in Fig. 5 and in the inset of Fig. 6. These data are quite similar to the traces in Fig. 4 but the magnitude of the dips is much larger. At the same separation and temperature ($L=30$ $\mu$m, $T=2$ K), the dips in BiPb (1) are about 30 times larger than those in Bi (26). All data sets show good qualitative agreement with the expected shape of a spin accumulation effect as derived from AMR data (refer to Fig. 4). The qualitative features reproduced well in two Bi samples, Bi (20) and Bi (26). Quantitatively, $\Delta R$ ($L=30$ $\mu$m) was about three times larger in Bi (20). Values of

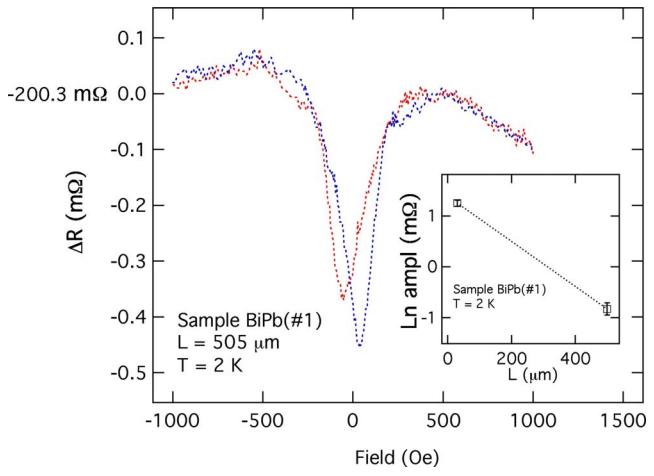


FIG. 5. (Color online) Example of spin accumulation data in sample BiPb(1). $T=2$ K. $L=505$ $\mu$m. Electrodes $F1$ and $F2_b$ [refer to Fig. 1(c)]. Blue: field sweep up. Red: field sweep down. The resistance at $H=0$ is $-0.2003$ $\Omega$ and $\Delta R$ is plotted. Inset: semilogarithmic plot of $\Delta R$ as a function of $L$.

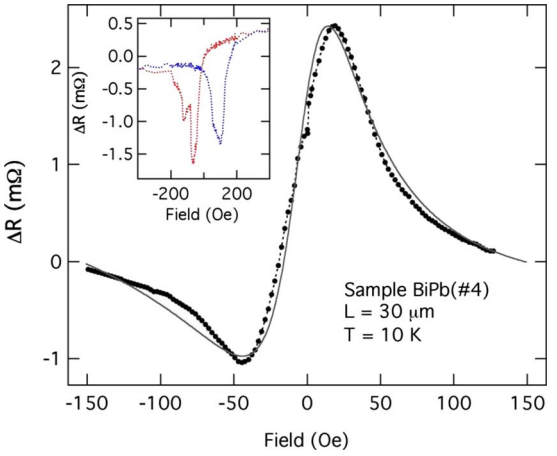


FIG. 6. (Color online) Spin accumulation in a BiPb film with semimetallic $\rho(T)$, detected by the Hanle effect. The fit (solid line) uses a mixture of absorptive and dispersive contributions, showing that **M1** and **M2** are not coplanar in the substrate plane. The resistance at $H=0$ is $R=0.966$ $\Omega$ and $\Delta R$ is plotted. Inset: spin accumulation data in a BiPb film, detected by magnetoresistance measurements. Sample BiPb (1), $T=10$ K, $L=30$ $\mu$m. Electrodes $F1$ and $F2_a$ [refer to Fig. 1(c)].

$\Delta R=2R_S$ for three probe separations of sample Bi (20) at $T=2$ K are shown as a semilogarithmic plot in the inset of Fig. 4. Fitting to Eq. (3) gives $\delta_{s,\mathrm{Bi}}=70\pm10$ $\mu$m. Data were taken at two-probe separations, $L=30$ $\mu$m and $L=505$ $\mu$m (Fig. 5), on sample BiPb (1) (set 2) in the temperature range of 2–10 K. The magnitude of $\delta_s$ diminished rapidly with increasing temperature; however an estimate of the spin diffusion length at $T=2$ K can be made from two data points, $\delta_{s,\mathrm{BiPb}}=230\pm30$ $\mu$m (Fig. 5, inset).

An example of the Hanle effect is shown with the data of Fig. 6. A large field, $H_y>500$ Oe, is applied along the $y$ axis [refer to Fig. 1(a)] in order to align both magnetizations **M1** and **M2** along $+\hat{y}$. After the field is reduced to zero, **M1** and **M2** remain approximately parallel in a remanent state. The voltage is then recorded as $H_x$ is swept along the $x$ axis. The asymmetric shape is characteristic of the Hanle effect when magnetizations **M1** and **M2** are not coplanar in the substrate plane. The solid line is a fit to the Bloch equations with a diffusion term.[25] The independent fitting parameters are $(1/\gamma T_2)=30$ Oe, $\delta_s=37$ $\mu$m, an amplitude factor discussed below, and the angle $\theta$ between **M1** and **M2**. By using the optimum combination of absorptive and dispersive contributions,[25] we find $\theta=42°$. It is likely that **M2**, composed of magnetically soft $Ni_{0.81}Fe_{0.19}$, lies along $y$. It is also likely that a few monolayers of Co oxidized at the substrate surface. Exchange coupling between $Co_{0.84}Fe_{0.16}$ could then result in a wide hysteresis loop (Fig. 3) along with a magnetization **M1** tilting upward toward $\hat{z}$.

Comparing Hanle effect data at $T=10$ K, BiPb (4), with MR data at 2 K, BiPb (1), we note that $\delta_s$ is shown to be sensitive to $T$, diminishing by a factor of 6 when $T$ is increased from 2 to 10 K. The decrease in $\delta_s(T)$ as $T$ increases, for BiPb, is not simply related to an increase in resistivity. In Bi (20), we find $\delta_s=70$ $\mu$m for a film with $\rho(2\ \mathrm{K})=7.5$ m$\Omega$ cm. By contrast, we find $\delta_s=39$ $\mu$m in BiPb (4), a

film with lower resistivity $\rho(10\ \mathrm{K})=1.0\ \mathrm{m}\Omega\ \mathrm{cm}$. This implies that $\delta_s$ is sensitive to both material composition and temperature.

## IV. DISCUSSION

We begin by noting that the spin diffusion lengths in both sample set 1, Bi films with semiconductorlike $\rho(T)$, and sample set 2, BiPb films characterized by semimetal-like $\rho(T)$, are extraordinarily long. To our knowledge, $\delta_{s,\mathrm{BiPb}}=230\pm30\ \mu\mathrm{m}$ is the longest spin diffusion length observed in any thin film sample. Our $\rho(T)$ and $R_H(T)$ measurements indicate that both electrons and holes contribute to charge and therefore spin and transport in both Bi and BiPb sample sets. These long spin diffusion lengths are undoubtedly related to the unusual transport properties of bismuth, but we know of no theory for spin dependent transport in group V materials.

Further analysis is instructive, and we compare data for Bi and BiPb samples at constant temperature, $T=2$ K. Using the Einstein relation, $\delta_s=\sqrt{D\tau_s}=[e^2\rho N(E_F)]^{-1/2}\sqrt{\tau_s}$, and measured values of $\delta_s$ and $\rho$ at 2 K, $\rho_{\mathrm{Bi}}=7.5\times10^{-3}\ \Omega\ \mathrm{cm}$ and $\rho_{\mathrm{BiPb}}=4.8\times10^{-4}\ \Omega\ \mathrm{cm}$, the measured ratio is

$$3.9\left[\frac{\tau_{s,\mathrm{BiPb}}}{\tau_{s,\mathrm{Bi}}}\frac{N(E_F)_{\mathrm{Bi}}}{N(E_F)_{\mathrm{BiPb}}}\right]^{1/2}=\frac{\delta_{s,\mathrm{BiPb}}}{\delta_{s,\mathrm{Bi}}}=\frac{230}{70}=3.3. \qquad (4)$$

Equation (4) shows that resistivity can account for the different spin diffusion lengths within about 15% and implies that the ratio $\tau_s/N(E_F)$ is the same for both Bi and BiPb sample sets at $T=2$ K. In other words, the spin diffusion length is diminished in sample set 1 [semiconductorlike $\rho(T)$] because the carrier diffusion constant is decreased relative to sample set 2 [semimetal-like $\rho(T)$].

Equation (2) can be used to estimate the polarization of current injected in BiPb. The approximate volume occupied by $\tilde{M}$ is the half disk [refer to Fig. 1(c)], $\mathcal{V}=\pi\delta_s^2 d$, and therefore $R_S=\eta_1\eta_2\rho/\pi d$. Using $R_S(L=30\ \mu\mathrm{m})=\Delta R/2=1.7\times10^{-3}\ \Omega$, the sole fitting parameter is the product $\eta_1\eta_2=1.0\times10^{-2}$, and the average value of interfacial polarization for BiPb (1) is $\eta_{\mathrm{av,BiPb}}=10\%$. Using the same volume to fit the magnitude of the Hanle effect in BiPb (4) at 10 K, we find $\eta_{\mathrm{av,BiPb}}=10.3\%$ and note that values of $\eta_{\mathrm{av,BiPb}}$ are in good agreement for different samples, different temperatures, and different measuring techniques. The spin accumulation in sample Bi (20) is smaller than that in BiPb (1) by a factor of about 12 ($L=30\ \mu\mathrm{m}$, $T=2$ K), and we estimate that the average fractional polarization is only about $\eta_{\mathrm{av,Bi}}=0.8\%$.

While differences in the spin diffusion length may be explained by differing resistivities of the materials, the reasons why $\eta_{\mathrm{av}}$ is 1 order of magnitude smaller for samples in set 1 are not clear but do not involve "resistance mismatch."[28] In the limit of zero interface resistance, the mismatch factor is[29]

$$M'=\frac{r_n}{r_f}(1-p_f^2), \qquad (5)$$

where $r_n$ ($r_f$) is the resistance of a length of a material equal to a spin depth in $N$ ($F$), $p_f$ is the fractional spin polarization in the bulk of $F$, and the observed polarization crossing the interface is the diminished value $\eta'=(1+M')^{-1}\eta$. Using $p_f=25\ \mu\Omega\ \mathrm{cm}$, $\delta_{s,f}=15$ nm,[22] and $p_f=0.5$, the mismatch factors are found to be $M'_{\mathrm{BiPb}}=2.3\times10^5$ for BiPb and $M'_{\mathrm{Bi}}=7.8\times10^5$ for Bi. These values are so large as to prohibit spin injection and detection entirely, and the observation of robust spin injection in four samples proves that the simple resistance mismatch model[28] is not relevant.[29]

In summary, we have measured spin injection, accumulation, and detection in samples of very similar materials, but three samples have temperature dependent resistivity characterized by semimetallic behavior and two others have $\rho(T)$ that show semiconducting behavior. The spin diffusion lengths are extraordinarily long; the value $\delta_{s,\mathrm{BiPb}}=230\ \mu\mathrm{m}$ is the longest spin depth observed in any thin film. The different values at constant temperature, $\delta_{s,\mathrm{BiPb}}\sim3\times\delta_{s,\mathrm{Bi}}$, can be explained by differences of resistivity and carrier diffusivity. However, an understanding of the origin of these long spin diffusion lengths requires a theory for spin dependent transport in semimetals. Such an understanding may offer another approach to the development of long spin diffusion lengths in other materials. We have further discovered that the fractional efficiency of spin injection/detection in Bi samples with semiconductorlike $\rho(T)$ is quite small, much less than the efficiency in nearly identical samples with semimetal-like $\rho(T)$. It can be noted that the interfacial spin transport efficiencies of injector and detector are assumed to be the same in nonmagnetic metal samples.[17] However, spin injected light emitting diodes (LEDs) show high fractional polarization for electrical injection from ferromagnetic metal electrodes.[30] It may follow that electrical detection is asymmetric and has low efficiency. Furthermore, the effective mass is different for carriers in metals and semiconductors, and changes in the carrier wave function, as the electrons cross the interface from metallic $F$ to semiconductor $N$, may not conserve spin.

## ACKNOWLEDGMENTS

This work was supported by a grant from the Fundamental R&D Program for Core Technology of Materials funded by the Ministry of Knowledge Economy, KOSEF through National Core Research Center for Nanomedical Technology, the Basic Research Program (R15–2004–024–00000–0), the Korea Research Foundation Grant funded by the Korean Government (MOEHRD, Basic Research Promotion Fund KRF-2007–314–C00107), the KIST Institutional Program and the TND Frontier Project funded by MEST. M.J. acknowledges the support of the Office of Naval Research through Grant No. N000-1405AF-00002.

*mark.b.johnson@nrl.navy.mil
†wooyoung@yonsei.ac.kr

[1] I. Žutić, J. Fabian, and S. Das Sarma, Rev. Mod. Phys. **76**, 323 (2004).
[2] S. D. Ganichev *et al.*, Nat. Phys. **2**, 609 (2006).
[3] S. S. P. Parkin, C. Kaiser, A. Panchula, P. M. Rice, B. Hughes, M. Samant, and S. H. Yang, Nature Mater. **3**, 862 (2004).
[4] P. Grunberg, J. Phys.: Condens. Matter **13**, 7691 (2001).
[5] S. Datta and B. Das, Appl. Phys. Lett. **56**, 665 (1990).
[6] S. A. Crooker, M. Furis, X. Lou, C. Adelmann, D. L. Smith, C. J. Palmstrom, and P. A. Crowell, Science **309**, 2191 (2005).
[7] I. Appelbaum, B. Huang, and D. J. Monsma, Nature (London) **447**, 295 (2007).
[8] X. Lou, C. Adelmann, S. A. Crooker, E. S. Garlid, J. Zhang, K. S. Madhukar Reddy, S. D. Flexner, C. J. Palmstrom, and P. A. Crowell, Nat. Phys. **3**, 197 (2007).
[9] J. J. Hall and S. H. Koenig, IBM J. Res. Dev. **8**, 241 (1964).
[10] Z. B. Zhang, X. Sun, M. S. Dresselhaus, J. Y. Ying, and J. Heremans, Phys. Rev. B **61**, 4850 (2000).
[11] A. B. Pippard, *Magnetoresistance in Metals* (Cambridge University Press, Cambridge, UK, 1989).
[12] X. Gonze, J.-P. Michenaud, and J.-P. Vigneron, Phys. Scr. **37**, 785 (1988).
[13] D. S. McLachlan, Phys. Rev. B **28**, 6821 (1983).
[14] F. Y. Yang, D. Liu, K. M. Hong, D. H. Reich, P. C. Searson, and C. L. Chien, Science **284**, 1335 (1999).
[15] R. Rosenbaum and T. Murphy, Physica B **346-347**, 296 (2004).
[16] H. Grabov, V. A. Komarov, and O. N. Uryupin, Proceedings of the 17th IEEE International Conference on Thermoelectrics, 1998 (unpublished), Vol. XX, p. 241.
[17] Mark Johnson and R. H. Silsbee, Phys. Rev. Lett. **55**, 1790 (1985).
[18] S. Garzon, I. Zutic, and R. A. Webb, Phys. Rev. Lett. **94**, 176601 (2005).
[19] Y. Ji, A. Hoffmann, J. E. Pearson, and S. D. Bader, Appl. Phys. Lett. **88**, 052509 (2006).
[20] R. Godfrey and M. Johnson, Phys. Rev. Lett. **96**, 136601 (2006).
[21] M. Urech, V. Korenivski, N. Poli, and D. B. Haviland, Nano Lett. **6**, 871 (2006).
[22] D. Beckmann, H. B. Weber, and H. v. Lohneysen, Phys. Rev. Lett. **93**, 197003 (2004).
[23] S. O. Valenzuela and M. Tinkham, Nature (London) **442**, 176 (2006).
[24] M. Johnson, J. Appl. Phys. **75**, 6714 (1994).
[25] M. Johnson and R. H. Silsbee, Phys. Rev. B **37**, 5326 (1988).
[26] M. Johnson and R. H. Silsbee, Phys. Rev. B **76**, 153107 (2007).
[27] F. Y. Yang, K. Liu, C. L. Chien, and P. C. Searson, Phys. Rev. Lett. **82**, 3328 (1999). Refer to Table I, where $\rho(5\ \mathrm{K}) = 0.18\ \mathrm{m}\Omega\ \mathrm{cm}$ for a 10 $\mu$m thick film grown by electrodeposition. Resistivity is highly sensitive to morphology, and it is reasonable that our highly polycrystalline, sputtered and patterned films, should have resistivity four times higher.
[28] G. Schmidt, D. Ferrand, L. W. Molenkamp, A. T. Filip, and B. J. van Wees, Phys. Rev. B **62**, R4790 (2000).
[29] M. Johnson and J. Byers, Phys. Rev. B **67**, 125112 (2003).
[30] H. J. Zhu, M. Ramsteiner, H. Kostial, M. Wassermeier, H. P. Schonherr, and K. H. Ploog, Phys. Rev. Lett. **87**, 016601 (2001).